GR-Athena++ Simulations of Spinning Binary Black Hole Mergers

Estuti Shukla[1,2], **Alireza Rashti**[1,2], **Rossella Gamba**[1,2,3], **David Radice**[1,2,4] **and Koustav Chandra**[1,2,5]

[1] Institute for Gravitation and the Cosmos, The Pennsylvania State University, University Park, PA 16802, USA

[2] Department of Physics, The Pennsylvania State University, University Park, PA 16802, USA

[3] Department of Physics, University of California, Berkeley, CA 94720, USA

[4] Department of Astronomy & Astrophysics, The Pennsylvania State University, University Park, PA 16802, USA

[5] Max Planck Institute for Gravitational Physics (Albert Einstein Institute), Am Mühlenberg 1, 14476 Potsdam, Germany

E-mail: `estuti@psu.edu`

Abstract. We present the second release of the `GR-Athena++` waveform catalog, comprising four new quasi-circular, non-precessing, spinning binary black hole simulations. These simulations are performed at high resolutions and represent a step toward generating high-fidelity gravitational waveforms that can eventually meet the accuracy requirements of upcoming next-generation detectors, including LISA, Cosmic Explorer, and Einstein Telescope. Gravitational waves are extracted at future null infinity ($\mathcal{I}^+$) using both Cauchy characteristic extraction and finite-radius extraction. For each simulation, we provide strain data across multiple resolutions and analyze waveform accuracy via convergence studies and self-mismatch analyses. The absolute phase and relative amplitude differences reach their largest values near the merger, while the smallest errors are of order $\mathcal{O}(10^{-2})$ and $\mathcal{O}(10^{-3})$, respectively. A self-mismatch analysis of the dominant $(2,2)$ mode yields mismatches between $\mathcal{O}(10^{-5})$ and $\mathcal{O}(10^{-7})$ for a total binary mass of $10^6 M_\odot$ over the frequency range $f \in [0.002, 0.1]$ Hz using LISA's noise curve. All waveforms are publicly available via `ScholarSphere`.

1. Introduction

Over the past decade, the direct detection of gravitational waves (GWs) has provided unprecedented insights into compact binary coalescences (CBCs)[1, 2] and enabled tests of general relativity (GR) in the strong-field regime (see e.g. Refs [3, 4, 5, 6] and references therein). As current GW detectors continue to improve in sensitivity [7, 8, 9, 10], along with the construction of next-generation (XG) ground-based detectors such as Cosmic Explorer (CE) [11, 12] and Einstein Telescope (ET) [13, 14], and future space-based missions including LISA [15], TianQin [16], DECIGO [17], Taiji [18], and LGWA [19], the demand for high-fidelity numerical relativity (NR) waveforms is expected to increase significantly [20, 21, 22, 23, 24, 25, 26]. Such waveforms are essential for matched filtering, constraining source parameters, and conducting fundamental tests of GR.

There are several publicly available NR waveform catalogs such as SXS [27], RIT [28], MAYA [29], BAM [30], and CoRE [31]. These catalogs comprise a wide range of binary configurations, including precessing, eccentric, and high mass ratio systems. They include binary black holes (BBHs), binary neutron stars (BNSs) and black hole-neutron stars (BHNSs) merger waveforms. Unfortunately, some of these catalogs only consist of publicly available waveforms at a single resolution. Our present work complements these efforts by focusing specifically on high-resolution, quasi-circular, non-precessing spinning binary black hole (BBH) mergers [32, 33, 34, 35], extending the scope of the initial `GR-Athena++` catalog [36]. For each configuration, we carry out multiple high-resolution simulations and perform self-convergence tests to assess the numerical accuracy of the generated waveforms. While clear convergence across different resolutions was not observed, these simulations were carried out at very high numerical resolutions. As such, this work constitutes a step toward producing high-fidelity waveforms suitable for the precision demands of next-generation GW detectors.

The paper is structured as follows. In Sec. 2, we provide a brief overview of the numerical simulations performed for this catalog, including details about `GR-Athena++` code, initial configuration parameters and the methods used for GW extraction. In Sec. 3, we present the results of various simulations, along with a convergence analysis of waveform phase and relative amplitude across different resolutions. We also present self-mismatch calculations between the highest-resolution waveform and its lower-resolution counterparts. In Sec. 4, we summarize our findings and discuss possible improvements and future directions. We adopt the standard convention of geometrized units, setting $G = c = 1$ throughout this work.

2. Numerical Simulations

2.1. GR-Athena++ Code

`GR-Athena++` is a high-performance computing code designed to solve non-linear, coupled Einstein field equations. It employs a sixth-order finite differencing (FD) scheme for spatial derivatives and a fourth-order Runge-Kutta scheme for time evolution, along with adaptive mesh refinement (AMR) [37, 38]. To simulate BBHs, `GR-Athena++` adopts the Z4c formulation of the Einstein equations [39, 40] and moving puncture gauge conditions [37]. All simulations are $\sim 3500M$ long, and required approximately 26 million core-hours in total to complete.

2.2. Simulation Configurations

The previous `GR-Athena++` catalog release [36] focused on non-spinning BBH simulations; the present work expands the catalog by including four new spinning, quasi-

Table 1. Binary black hole configurations. ID is the identification number for the binary in the GR-Athena++ catalog. q is the mass ratio, D is the distance between the two black holes, χ_1 and χ_2 are the dimensionless spin values in the z direction for the two black holes. $|P_x/M|$ and $|P_y/M|$, respectively, denote the x and y momentum components of the black hole in the TwoPunctures initial data code. The total mass of the system is set to $M = 1$ in all cases. N is the number of grid points on the root grid in each spatial direction, while h indicates the grid resolutions at the finest level.

ID	q	χ_1	χ_2	D/M	$10^4\|P_x/M\|$	$10^2\|P_y/M\|$	N	$10^3 h/M$
0005	1.5	-0.1	0.1	13.5	3.974	7.574	128, 192, 256	14.47, 9.644, 7.233
0006	1.5	0.1	0.1	13	3.591	7.715	128, 192, 256, 320, 384	14.28, 6.877, 7.141, 5.713, 4.761
0007	1.5	-0.4	0.4	13.5	3.381	7.6	128, 192, 256, 320, 384	15.26, 7.365, 7.629, 6.104, 5.086
0008	1.5	0.4	0.4	12.5	2.826	7.787	128, 192, 256, 320, 384	13.49, 6.632, 6.744, 5.396, 4.496

circular BBH configurations as detailed in Table 1. All configurations have a mass ratio $q = m_1/m_2 = 1.5$ where $m_1 \geq m_2$, and the total mass of the binary system $(m_1 + m_2)$ is fixed at 1. Owing to the scale invariance of the vacuum Einstein field equations, the total mass can be fixed without loss of generality. The parameters chosen for these configurations make them suitable not only for informing waveform models of BBHs, but also for providing robust point-mass baselines for the construction of models for GWs from BNSs and BHNSs [41, 42, 43, 44, 45].

The two BHs are initially placed in the xy-plane separated by a distance D with linear momentum P_x and P_y (specified in Table 1). The evolution is carried out only for $z > 0$, with bitant symmetry imposed at $z = 0$ to take advantage of the reflection symmetry across the orbital plane. Simulations with ID 0006-0008 are carried out at five levels of grid resolution, with N denoting the number of grid points on the root grid in each spatial direction. For ID 0005, only three resolutions are available. The initial data is prepared using the TwoPunctures code [46], followed by an eccentricity reduction procedure [47] to get low-eccentricity orbits. This step is critical to achieve quasi-circular inspiral during the last phases before merger, generating roughly 25 pre-merger cycles. The orbital eccentricities measured 1200M before merger are approximately $\sim 8 \times 10^{-4}$ for ID 0006, $\sim 2 \times 10^{-4}$ for ID 0008 (aligned-spin cases), and $\sim 6 \times 10^{-4}$ for ID 0005, $\sim 1 \times 10^{-3}$ for ID 0007 (contra-aligned-spin cases). We use the gw_eccentricity package [48, 49] to estimate the orbital eccentricities of these simulations from the finite-radius waveforms generated by GR-Athena++.

2.3. Waveform Extraction

We extract GWs from BBH mergers at future null infinity ($\mathcal{I}^+$) using two methods. The first method is finite-radius extraction (FRE) [50, 51], which extrapolates waveforms computed at finite-radius to $\mathcal{I}^+$. This approximation method relies on a perturbative, post-Newtonian-inspired expansion. The second method, Cauchy characteristic extraction (CCE) [52], uses a characteristic evolution scheme to propagate data from a finite-radius worldtube to $\mathcal{I}^+$. Unlike FRE, this approach incorporates the full nonlinear structure of the spacetime [53] in the characteristic domain and yields more accurate waveforms. The required worldtube initial data is provided by `GR-Athena++` and we perform CCE using `PITTNuLL` code [54, 53], which outputs the waveform as Weyl scalar (Ψ_4). The complex GW strain (h) is calculated from $\Psi_4 = \ddot{h}_+ - i\ddot{h}_\times$ using fixed-frequency integration (FFI) [55]. We refer the readers to [36] for further details on the methodology and implementation. Our waveforms do not make use of the newly developed infrastructure for waveform extraction based on the Regge-Zerilli-Wheeler formalism, which was recently added to `GR-Athena++` [56, 57], but was not available at the time we performed the simulations reported here.

3. Results

3.1. Gravitational Waveforms

We simulate BBH mergers with four different spin configurations using `GR-Athena++` at multiple high resolutions. GW strains are extracted via CCE from worldtube data at radius $R = 50$, and via FRE at coordinate radii $R = 60$, 80, 100, 120, and 140. For simulation `ID 0005`, only FRE waveforms are available. For consistency, all subsequent analysis is done with FRE waveforms extracted at $R = 100$.

In Figure 1, we show the real and imaginary part of $(\ell, m) = (2, 2)$ mode of the complex GW strain $h = h_+ - ih_\times$ from the highest-resolution runs for each binary. We observe the characteristic phases of a binary black-hole coalescence: an inspiral phase, followed by a merger—where the waveform amplitude reaches its peak—and a subsequent ringdown. Since these systems have low eccentricities, we expect minimal oscillations in the amplitude, consistent with what is observed in the figure. In Figure 2, we show (ℓ, m) modes—(2,2), (2,1), (3,2), (3,3), (4,4), and (5,5) for `ID 0008` ($\chi_1 = 0.4$, $\chi_2 = 0.4$). Owing to reflection symmetry, these modes satisfy $h_{\ell,-m} = (-1)^\ell h^*_{\ell m}$, and in our simulations, the $-m$ modes exhibit morphological and phase evolution consistency with their corresponding $m > 0$ counterparts. As expected, the $(\ell, m) = (2, 2)$ is the dominant mode. Qualitatively, the higher harmonic modes exhibit physically consistent behavior and do not appear to be dominated by numerical noise. These subdominant modes are expected to play an important role for XG detectors [58].

3.2. Error Analysis

To assess the numerical accuracy of our simulations, we perform a convergence analysis by comparing waveforms at different grid resolutions against the highest-resolution simulation for each configuration. Figures 3 and 4 present the absolute phase differences and relative amplitude differences, respectively, between each lower-resolution run and its corresponding highest-resolution counterpart. In both cases, we observe that these differences increase as the system approaches merger, with the largest discrepancies occurring near the merger time, which is defined as the peak amplitude of dominant $(2, 2)$ mode. This is an expected trend because errors accumulate during the evolution

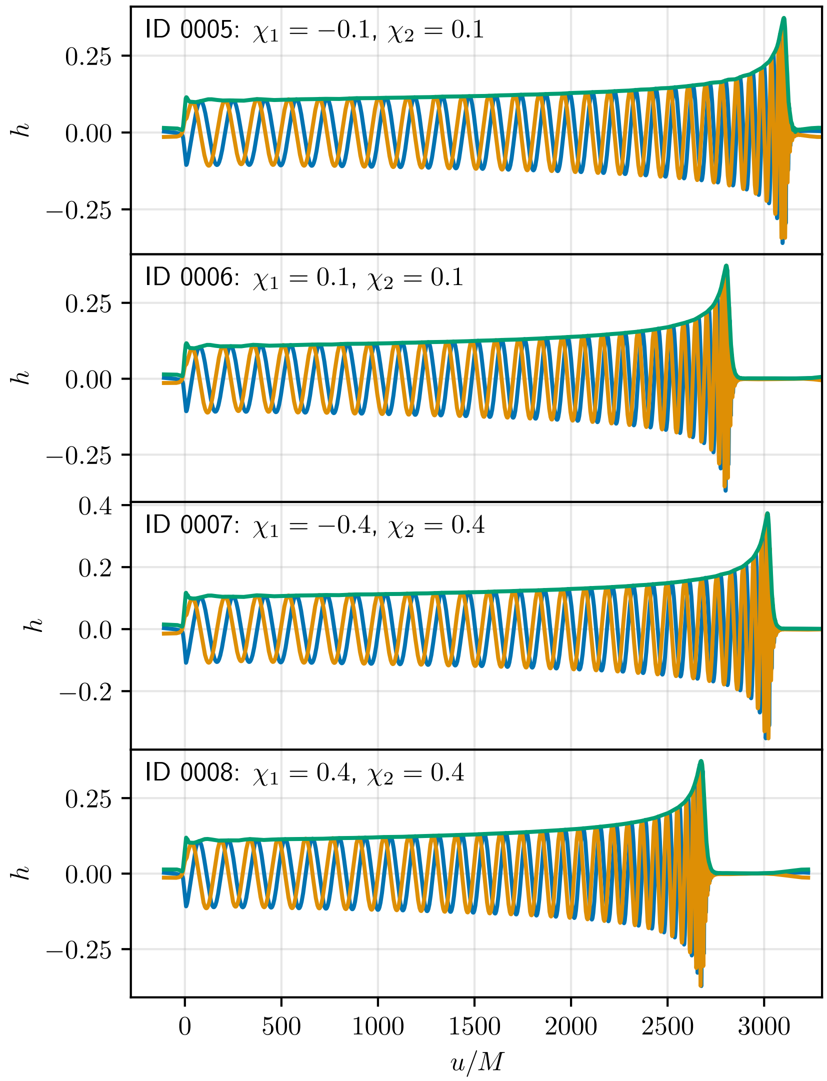

Figure 1. GW strains for the dominant $(\ell, m) = (2, 2)$ mode from the highest-resolution simulations of four binary black hole systems. Each panel displays the real part (blue), imaginary part (orange), and amplitude (green) of the complex strain $h = h_+ - ih_\times$ as a function of retarded time u/M. The simulations differ in their spin configurations: `ID 0005` ($\chi_1 = -0.1$, $\chi_2 = 0.1$), `ID 0006` ($\chi_1 = 0.1$, $\chi_2 = 0.1$), `ID 0007` ($\chi_1 = -0.4$, $\chi_2 = 0.4$), and `ID 0008` ($\chi_1 = 0.4$, $\chi_2 = 0.4$). All these waveforms are calculated using FRE.

of the binary. We do not observe convergence at a fixed polynomial order. However, the differences in phase and relative amplitude decrease with resolution. Our waveforms at merger exhibit dephasing as small as $\mathcal{O}(10^{-2})$ and relative amplitude differences of $\mathcal{O}(10^{-3})$.

In Figure 5, we quantify the agreement between the highest-resolution waveform and its lower-resolution counterparts for a given simulation by computing the self-mismatch

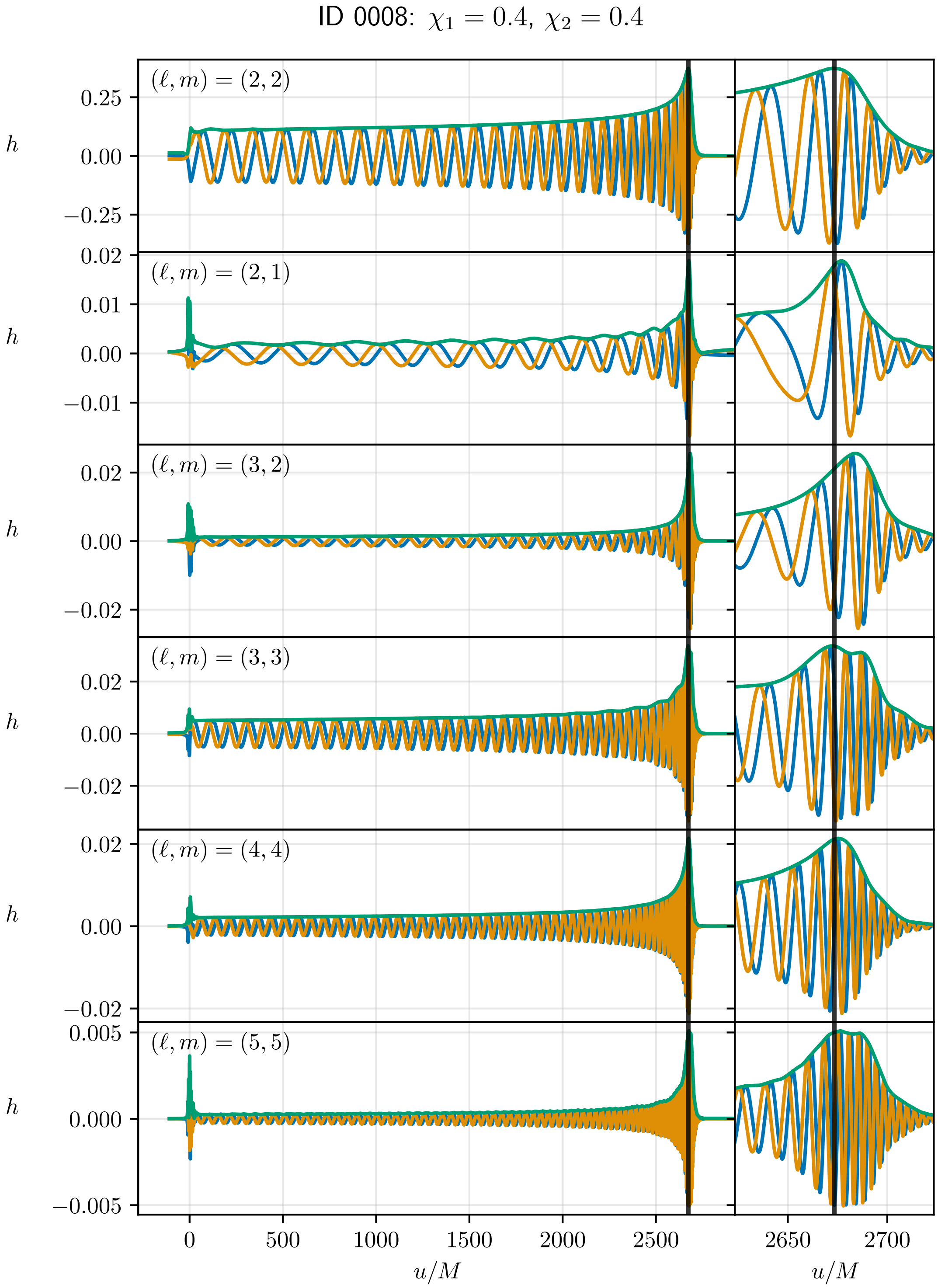

Figure 2. Highest-resolution GW strains for the spin configuration `ID 0008` ($\chi_1 = 0.4$, $\chi_2 = 0.4$), showing various (ℓ, m) modes—(2,2), (2,1), (3,2), (3,3), (4,4), and (5,5)—as a function of retarded time u/M. Each panel displays the real part (blue), imaginary part (orange), and amplitude (green) of the complex strain. The vertical black lines mark the merger time, defined as the time of maximum amplitude of the dominant (2,2) mode. The side panel displays the zoom-in around the merger time.

($\bar{\mathcal{M}}$), defined as

$$\bar{\mathcal{M}}(h, h') = 1 - \max_{\Delta\phi\Delta t} \mathcal{O}(h, h'), \tag{1}$$

where h and h' denote two Fourier-domain waveforms corresponding to the dominant $(2, 2)$ mode, and the overlap $\mathcal{O}(h, h')$ is maximized over an arbitrary phase difference $\Delta\phi$ and time shift Δt [59, 60]. For this calculation, we use the LISA noise curve from [61] and fix the total mass of the binary to $10^6 M_\odot$. The initial and final frequencies are taken to be 2×10^{-3} Hz and 0.1 Hz respectively, ensuring that merger happens within the frequency band of the detector. We observe that the trend in mismatch values is consistent with the dephasing behavior shown in Figure 3 and lies between $\mathcal{O}(10^{-5})$ to $\mathcal{O}(10^{-7})$ for various simulations. Notably, the N320 resolution run for `ID 0006` attains a mismatch lower than 10^{-7}. For LISA, we expect to observe signals with signal-to-noise ratio (SNR) as high as 1000, which demand waveform accuracies with mismatches of the order of $\mathcal{O}(10^{-7})$. These are among the highest-resolution spinning, quasi-circular simulations carried out with a FD code.

4. Conclusion and Discussions

We performed four configurations of non-precessing, spinning, quasi-circular BBH mergers using `GR-Athena++` at multiple high resolutions. The initial data for these runs was generated using the `TwoPunctures` code. As summarized in Table 1, the configurations included two aligned-spin and two contra-aligned-spin BBH systems, and constitute the second set of simulations released as part of the `GR-Athena++` waveform catalog [32, 33, 34, 35]. GW strains were extracted at future null infinity ($\mathcal{I}^+$) using both CCE, via the `PITTNull` code, and FRE. To assess the quality of the waveforms, we performed a convergence analysis by comparing the dominant $(2, 2)$ strain modes across different grid resolutions, using the highest-resolution FRE waveform for each configuration as a reference. Near the merger, the absolute phase and relative amplitude differences reach their maximum values, while their smallest deviations are $\mathcal{O}(10^{-2})$ and $\mathcal{O}(10^{-3})$, respectively. Although we do not observe clean convergence at a fixed polynomial order, we observe a general decrease in the phase and relative amplitude differences with resolution. We also computed the self-mismatch for each run between the highest-resolution available and its lower-resolution counterparts using the (2,2) mode. The general behavior of the mismatch values closely follows the trends observed in the phase convergence analysis and lies in the range between $\mathcal{O}(10^{-5})$ to $\mathcal{O}(10^{-7})$. Conducted at some of the highest resolutions achieved with a FD code, these spinning, quasi-circular simulations yield waveforms that can be used to calibrate and validate semi-analytical GW models and benchmark against existing NR catalogs.

Future addition to the `GR-Athena++` catalog will be produced using the GPU version of our code, based on `AthenaK` [62]. In particular, we plan to expand the `GR-Athena++` catalog to include eccentric, precessing, and higher mass ratio BBH runs.

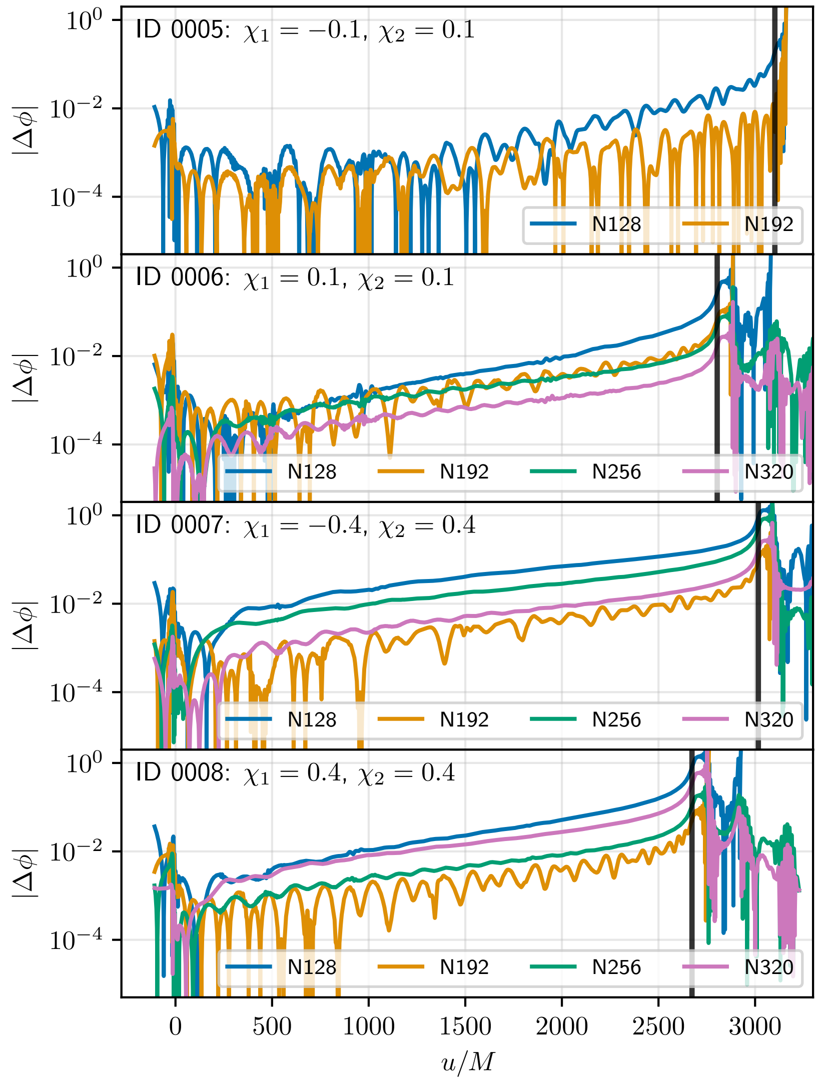

Figure 3. Convergence study of strains using FRE waveforms. We show the absolute phase differences $|\Delta\phi|$ between different numerical resolutions and the highest-resolution simulation for $(\ell, m) = (2, 2)$ mode as a function of retarded time u/M. The vertical black lines mark the merger time.

Data Availability Statement

All data supporting our findings is available through `ScholarSphere` [32, 33, 34, 35].

Acknowledgments

`Claude.ai` was used in preparing the data plotting scripts. This work was supported by NASA under Award No. 80NSSC21K1720. RG acknowledges support from NSF Grant PHY-2020275 (Network for Neutrinos, Nuclear Astrophysics, and Symmetries (N3AS)). KC acknowledges the generous support from NSF grants PHY-2207638, AST-2307147,

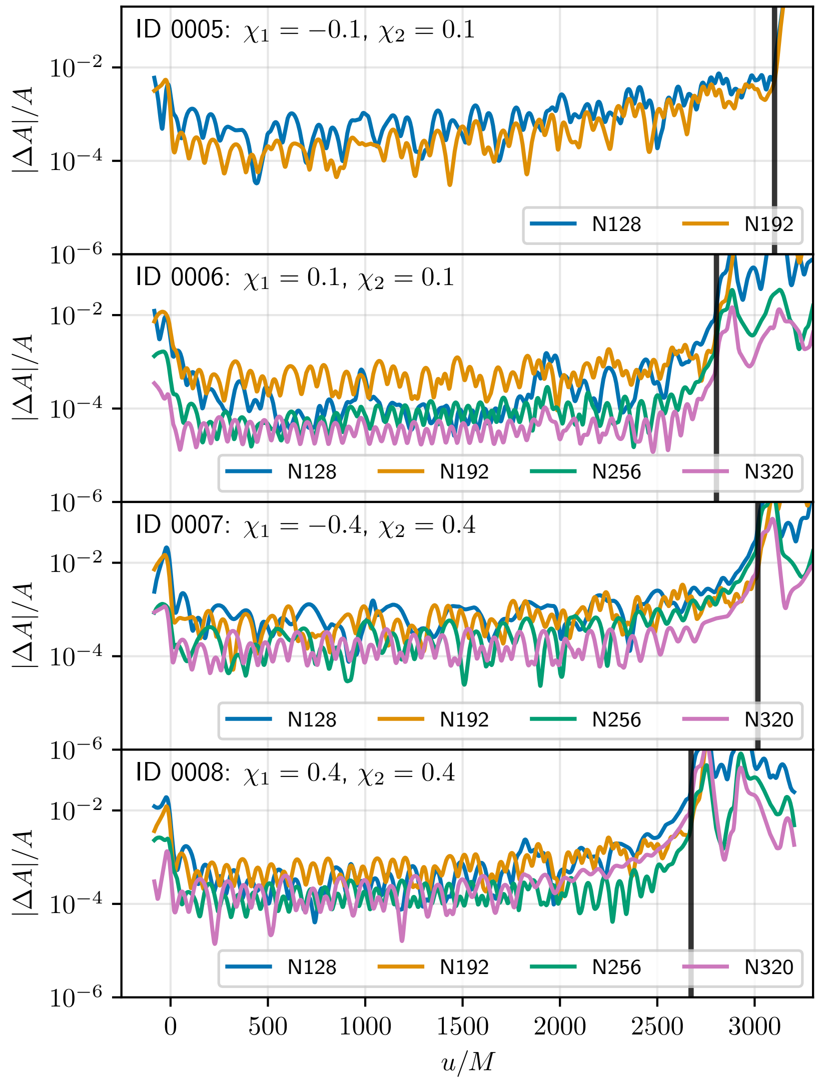

Figure 4. Convergence study of strains using FRE waveform. We show the relative amplitude differences $|\Delta A|/A$ between different numerical resolutions and the highest-resolution simulation for $(\ell, m) = (2, 2)$ mode. The vertical black lines mark the merger time. The amplitude differences have been smoothed with a $50M$ window to reduce numerical noise.

PHY-2308886, and PHY-2309064. Simulations were performed on Frontera (NSF LRAC allocation PHY23001)

References

[1] A. G. Abac et al. "GWTC-4.0: Updating the Gravitational-Wave Transient Catalog with Observations from the First Part of the Fourth LIGO-Virgo-KAGRA Observing Run". In: (Aug. 2025). arXiv: `2508.18082 [gr-qc]`.

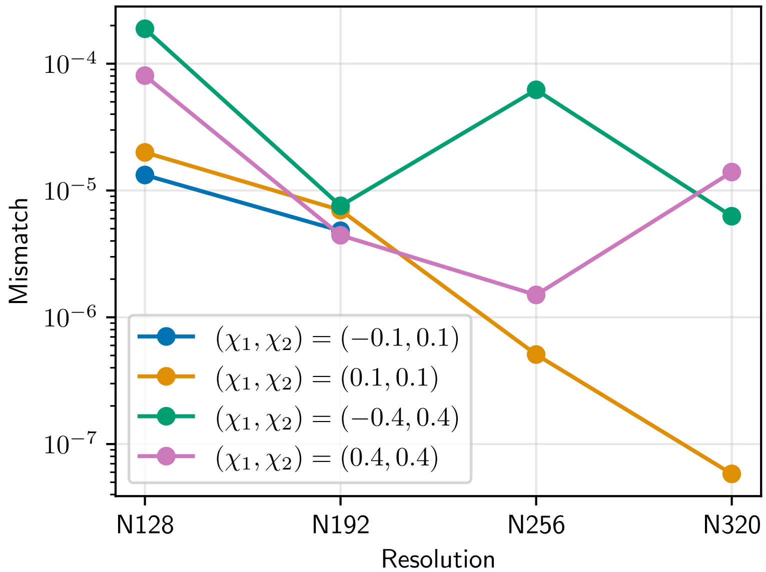

Figure 5. Self-mismatch study using $(\ell, m) = (2, 2)$ mode of FRE waveforms. We compute the self-mismatch (Eq. 1) between the highest-resolution run and its lower-resolution counterparts for each simulation using LISA noise curve. We set the total mass of the binary as $10^6 M_\odot$ and calculate mismatch within the frequency band $f \in [0.002, 0.1]$ Hz.

[2] A. G. Abac et al. "GWTC-4.0: Population Properties of Merging Compact Binaries". In: (Aug. 2025). arXiv: 2508.18083 [astro-ph.HE].

[3] "Black Hole Spectroscopy and Tests of General Relativity with GW250114". In: (Sept. 2025). arXiv: 2509.08099 [gr-qc].

[4] R. Abbott et al. "Tests of General Relativity with GWTC-3". In: (Dec. 2021). arXiv: 2112.06861 [gr-qc].

[5] Nicolas Yunes, Xavier Siemens, and Kent Yagi. "Gravitational-Wave Tests of General Relativity with Ground-Based Detectors and Pulsar-Timing Arrays". In: (Aug. 2024). arXiv: 2408.05240 [gr-qc].

[6] N. V. Krishnendu and Frank Ohme. "Testing General Relativity with Gravitational Waves: An Overview". In: *Universe* 7.12 (2021), p. 497. DOI: 10.3390/universe7120497. arXiv: 2201.05418 [gr-qc].

[7] T. Akutsu et al. "Overview of KAGRA: Detector design and construction history". In: *PTEP* 2021.5 (2021), 05A101. DOI: 10.1093/ptep/ptaa125. arXiv: 2005.05574 [physics.ins-det].

[8] B. P. Abbott et al. "Prospects for observing and localizing gravitational-wave transients with Advanced LIGO, Advanced Virgo and KAGRA". In: *Living Rev. Rel.* 19 (2016), p. 1. DOI: 10.1007/s41114-020-00026-9. arXiv: 1304.0670 [gr-qc].

[9] J. Aasi et al. "Advanced LIGO". In: *Class. Quant. Grav.* 32 (2015), p. 074001. DOI: 10.1088/0264-9381/32/7/074001. arXiv: 1411.4547 [gr-qc].

[10] F. Acernese et al. "Advanced Virgo: a second-generation interferometric gravitational wave detector". In: *Class. Quant. Grav.* 32.2 (2015), p. 024001. DOI: 10.1088/0264-9381/32/2/024001. arXiv: 1408.3978 [gr-qc].

[11] David Reitze et al. "Cosmic Explorer: The U.S. Contribution to Gravitational-Wave Astronomy beyond LIGO". In: *Bull. Am. Astron. Soc.* 51.7 (2019), p. 035. arXiv: 1907.04833 [astro-ph.IM].

[12] Matthew Evans et al. "A Horizon Study for Cosmic Explorer: Science, Observatories, and Community". In: (Sept. 2021). arXiv: 2109.09882 [astro-ph.IM].

[13] M. Punturo et al. "The Einstein Telescope: A third-generation gravitational wave observatory". In: *Class. Quant. Grav.* 27 (2010). Ed. by Fulvio Ricci, p. 194002. DOI: 10.1088/0264-9381/27/19/194002.

[14] Michele Maggiore et al. "Science Case for the Einstein Telescope". In: *JCAP* 03 (2020), p. 050. DOI: 10.1088/1475-7516/2020/03/050. arXiv: 1912.02622 [astro-ph.CO].

[15] Pau Amaro-Seoane et al. "Laser Interferometer Space Antenna". In: *arXiv e-prints*, arXiv:1702.00786 (Feb. 2017), arXiv:1702.00786. DOI: 10.48550/arXiv.1702.00786. arXiv: 1702.00786 [astro-ph.IM].

[16] Jun Luo et al. "TianQin: a space-borne gravitational wave detector". In: *Class. Quant. Grav.* 33.3 (2016), p. 035010. DOI: 10.1088/0264-9381/33/3/035010. arXiv: 1512.02076 [astro-ph.IM].

[17] S. Kawamura et al. "The Japanese space gravitational wave antenna DECIGO". In: *Class. Quant. Grav.* 23 (2006). Ed. by N. Mio, S125–S132. DOI: 10.1088/0264-9381/23/8/S17.

[18] Ziren Luo et al. "A brief analysis to Taiji: Science and technology". In: *Results Phys.* 16 (2020), p. 102918. DOI: 10.1016/j.rinp.2019.102918.

[19] Parameswaran Ajith et al. "The Lunar Gravitational-wave Antenna: mission studies and science case". In: *JCAP* 01 (2025), p. 108. DOI: 10.1088/1475-7516/2025/01/108. arXiv: 2404.09181 [gr-qc].

[20] Lee Lindblom, Benjamin J. Owen, and Duncan A. Brown. "Model Waveform Accuracy Standards for Gravitational Wave Data Analysis". In: *Phys. Rev. D* 78 (2008), p. 124020. DOI: 10.1103/PhysRevD.78.124020. arXiv: 0809.3844 [gr-qc].

[21] Veome Kapil et al. "Systematic bias from waveform modeling for binary black hole populations in next-generation gravitational wave detectors". In: *Phys. Rev. D* 109.10 (2024), p. 104043. DOI: 10.1103/PhysRevD.109.104043. arXiv: 2404.00090 [gr-qc].

[22] Arnab Dhani et al. "Systematic Biases in Estimating the Properties of Black Holes Due to Inaccurate Gravitational-Wave Models". In: *Phys. Rev. X* 15.3 (2025), p. 031036. DOI: 10.1103/5pks-qz6b. arXiv: 2404.05811 [gr-qc].

[23] Michael Pürrer and Carl-Johan Haster. "Gravitational waveform accuracy requirements for future ground-based detectors". In: *Phys. Rev. Res.* 2.2 (2020), p. 023151. DOI: 10.1103/PhysRevResearch.2.023151. arXiv: 1912.10055 [gr-qc].

[24] Aasim Jan et al. "Accuracy limitations of existing numerical relativity waveforms on the data analysis of current and future ground-based detectors". In: *Phys. Rev. D* 110.2 (2024), p. 024023. DOI: 10.1103/PhysRevD.110.024023. arXiv: 2312.10241 [gr-qc].

[25] Deborah Ferguson et al. "Assessing the readiness of numerical relativity for LISA and 3G detectors". In: *Phys. Rev. D* 104.4 (2021), p. 044037. DOI: 10.1103/PhysRevD.104.044037. arXiv: 2006.04272 [gr-qc].

[26] Koustav Chandra. "gwforge: a user-friendly package to generate gravitational-wave mock data". In: *Class. Quant. Grav.* 42.2 (2025), p. 025003. DOI: 10.1088/1361-6382/ad9b68. arXiv: 2407.21109 [gr-qc].

[27] Mark A. Scheel et al. "The SXS collaboration's third catalog of binary black hole simulations". In: *Class. Quant. Grav.* 42.19 (2025), p. 195017. DOI: 10.1088/1361-6382/adfd34. arXiv: 2505.13378 [gr-qc].

[28] James Healy and Carlos O. Lousto. "Fourth RIT binary black hole simulations catalog: Extension to eccentric orbits". In: *Phys. Rev. D* 105.12 (2022), p. 124010. DOI: 10.1103/PhysRevD.105.124010. arXiv: 2202.00018 [gr-qc].

[29] Deborah Ferguson et al. "Second MAYA catalog of binary black hole numerical relativity waveforms". In: *Phys. Rev. D* 112.4 (2025), p. 044043. DOI: 10.1103/gk7x-9cds. arXiv: 2309.00262 [gr-qc].

[30] Eleanor Hamilton et al. "Catalog of precessing black-hole-binary numerical-relativity simulations". In: *Phys. Rev. D* 109.4 (2024), p. 044032. DOI: 10.1103/PhysRevD.109.044032. arXiv: 2303.05419 [gr-qc].

[31] Alejandra Gonzalez et al. "Second release of the CoRe database of binary neutron star merger waveforms". In: *Class. Quant. Grav.* 40.8 (2023), p. 085011. DOI: 10.1088/1361-6382/acc231. arXiv: 2210.16366 [gr-qc].

[32] David Radice and Alireza Rashti. *GRAthena:BHBH:0005*. Dataset release. 2025. DOI: 10.26207/zsps-ar14. URL: https://doi.org/10.26207/zsps-ar14.

[33] David Radice and Alireza Rashti. *GRAthena:BHBH:0006*. Dataset release. 2025. DOI: 10.26207/azq0-fd42. URL: https://doi.org/10.26207/azq0-fd42.

[34] David Radice and Alireza Rashti. *GRAthena:BHBH:0007*. Dataset release. 2025. DOI: 10.26207/1dav-8v37. URL: https://doi.org/10.26207/1dav-8v37.

[35] David Radice and Alireza Rashti. *GRAthena:BHBH:0008*. Dataset release. 2025. DOI: 10.26207/r4d8-2c27. URL: https://doi.org/10.26207/r4d8-2c27.

[36] Alireza Rashti et al. "Binary black hole waveforms from high-resolution gr-athena++ simulations". In: *Phys. Rev. D* 111.10 (2025), p. 104078. DOI: 10.1103/n5pz-qv3x. arXiv: 2411.11989 [gr-qc].

[37] Boris Daszuta et al. "GR-Athena++: Puncture Evolutions on Vertex-centered Oct-tree Adaptive Mesh Refinement". In: *Astrophys. J. Supp.* 257.2 (2021), p. 25. DOI: 10.3847/1538-4365/ac157b. arXiv: 2101.08289 [gr-qc].

[38] Alireza Rashti et al. "Adaptive mesh refinement in binary black holes simulations". In: *Class. Quant. Grav.* 41.9 (2024), p. 095001. DOI: 10.1088/1361-6382/ad36a5. arXiv: 2312.05438 [gr-qc].

[39] David Hilditch et al. "Compact binary evolutions with the Z4c formulation". In: *Phys. Rev. D* 88 (2013), p. 084057. DOI: 10.1103/PhysRevD.88.084057. arXiv: 1212.2901 [gr-qc].

[40] Sebastiano Bernuzzi and David Hilditch. "Constraint violation in free evolution schemes: Comparing BSSNOK with a conformal decomposition of Z4". In: *Phys. Rev. D* 81 (2010), p. 084003. DOI: 10.1103/PhysRevD.81.084003. arXiv: 0912.2920 [gr-qc].

[41] Jonathan E. Thompson et al. "Modeling the gravitational wave signature of neutron star black hole coalescences". In: *Phys. Rev. D* 101.12 (2020), p. 124059. DOI: 10.1103/PhysRevD.101.124059. arXiv: 2002.08383 [gr-qc].

[42] Rossella Gamba et al. "Analytically improved and numerical-relativity informed effective-one-body model for coalescing binary neutron stars". In: (July 2023). arXiv: 2307.15125 [gr-qc].

[43] Adrian Abac et al. "New and robust gravitational-waveform model for high-mass-ratio binary neutron star systems with dynamical tidal effects". In: *Phys. Rev. D* 109.2 (2024), p. 024062. DOI: 10.1103/PhysRevD.109.024062. arXiv: 2311.07456 [gr-qc].

[44] Marcus Haberland, Alessandra Buonanno, and Jan Steinhoff. "Modeling matter in seobnrv5thm: Generating fast and accurate effective-one-body waveforms for spin-aligned binary neutron stars". In: *Phys. Rev. D* 112.8 (2025), p. 084024. DOI: 10.1103/d3ns-h77x. arXiv: 2503.18934 [gr-qc].

[45] Alejandra Gonzalez et al. "Black-hole - neutron-star mergers: new numerical-relativity simulations and multipolar effective-one-body model with spin precession and eccentricity". In: (June 2025). arXiv: 2507.00113 [gr-qc].

[46] Marcus Ansorg, Bernd Bruegmann, and Wolfgang Tichy. "A Single-domain spectral method for black hole puncture data". In: *Phys. Rev. D* 70 (2004), p. 064011. DOI: 10.1103/PhysRevD.70.064011. arXiv: gr-qc/0404056.

[47] Antoni Ramos-Buades, Sascha Husa, and Geraint Pratten. "Simple procedures to reduce eccentricity of binary black hole simulations". In: *Phys. Rev. D* 99.2 (2019), p. 023003. DOI: 10.1103/PhysRevD.99.023003. arXiv: 1810.00036 [gr-qc].

[48] Md Arif Shaikh et al. "Defining eccentricity for gravitational wave astronomy". In: *Phys. Rev. D* 108.10 (2023), p. 104007. DOI: 10.1103/PhysRevD.108.104007. arXiv: 2302.11257 [gr-qc].

[49] Md Arif Shaikh et al. "Defining eccentricity for spin-precessing binaries". In: *Class. Quant. Grav.* 42.19 (2025), p. 195012. DOI: 10.1088/1361-6382/ae085d. arXiv: 2507.08345 [gr-qc].

[50] Carlos O. Lousto et al. "Intermediate-mass-ratio black hole binaries: Intertwining numerical and perturbative techniques". In: *Phys. Rev. D* 82 (2010), p. 104057. DOI: 10.1103/PhysRevD.82.104057. arXiv: 1008.4360 [gr-qc].

[51] Kenta Kiuchi et al. "Sub-radian-accuracy gravitational waveforms of coalescing binary neutron stars in numerical relativity". In: *Phys. Rev. D* 96.8 (2017), p. 084060. DOI: 10.1103/PhysRevD.96.084060. arXiv: 1708.08926 [astro-ph.HE].

[52] Nigel T. Bishop et al. "Cauchy-characteristic extraction in numerical relativity". In: *Phys. Rev. D* 54 (1996), pp. 6153–6165. DOI: 10.1103/PhysRevD.54.6153. arXiv: gr-qc/9705033.

[53] Nigel T. Bishop et al. "Cauchy characteristic matching". In: *Black Holes, Gravitational Radiation and the Universe: Essays in Honor of C.V. Vishveshwara.* Ed. by Bala R. Iyer and B. Bhawal. Jan. 1998, pp. 383–408. DOI: 10.1007/978-94-017-0934-7_24. arXiv: gr-qc/9801070.

[54] M. C. Babiuc et al. "A Characteristic Extraction Tool for Gravitational Waveforms". In: *Phys. Rev. D* 84 (2011), p. 044057. DOI: 10.1103/PhysRevD.84.044057. arXiv: 1011.4223 [gr-qc].

[55] Christian Reisswig and Denis Pollney. "Notes on the integration of numerical relativity waveforms". In: *Class. Quant. Grav.* 28 (2011), p. 195015. DOI: 10.1088/0264-9381/28/19/195015. arXiv: 1006.1632 [gr-qc].

[56] Joan Fontbuté et al. "Covariant and Gauge-invariant Metric-based Gravitational-waves Extraction in Numerical Relativity". In: (Aug. 2025). arXiv: 2508.03799 [gr-qc].

[57] Sebastiano Bernuzzi et al. "Perturbative Hyperboloidal Extraction of Gravitational Waves in 3+1 Numerical Relativity". In: (Aug. 2025). arXiv: 2508.05743 [gr-qc].

[58] Divyajyoti et al. "Detectability of gravitational higher order modes in the third-generation era". In: *Phys. Rev. D* 104.8 (2021), p. 084080. DOI: 10.1103/PhysRevD.104.084080. arXiv: 2103.03241 [gr-qc].

[59] B. S. Sathyaprakash and S. V. Dhurandhar. "Choice of filters for the detection of gravitational waves from coalescing binaries". In: *Phys. Rev. D* 44 (1991), pp. 3819–3834. DOI: 10.1103/PhysRevD.44.3819.

[60] Benjamin J. Owen. "Search templates for gravitational waves from inspiraling binaries: Choice of template spacing". In: *Phys. Rev. D* 53 (1996), pp. 6749–6761. DOI: 10.1103/PhysRevD.53.6749. arXiv: gr-qc/9511032.

[61] Stanislav Babak, Antoine Petiteau, and Martin Hewitson. "LISA Sensitivity and SNR Calculations". In: (Aug. 2021). arXiv: 2108.01167 [astro-ph.IM].

[62] Hengrui Zhu et al. “Performance-portable Numerical Relativity with AthenaK”. In: *Astrophys. J. Suppl.* 278.2 (2025), p. 50. DOI: 10.3847/1538-4365/adcf96. arXiv: 2409.10383 [gr-qc].